SUPRAMOLECULAR CHEMISTRY

Structural water as an essential comonomer in supramolecular polymerization

Shengyi Dong,[1]* Jing Leng,[2] Yexin Feng,[3] Ming Liu,[4] Chloe J. Stackhouse,[4] Andreas Schönhals,[2] Leonardo Chiappisi,[5,6] Lingyan Gao,[7] Wei Chen,[8] Jie Shang,[9] Lin Jin,[9] Zhenhui Qi,[9]* Christoph A. Schalley[7,9]*

Although the concept of structural water that is bound inside hydrophobic pockets and helps to stabilize protein structures is well established, water has rarely found a similar role in supramolecular polymers. Water is often used as a solvent for supramolecular polymerization, however without taking the role of a comonomer for the supramolecular polymer structure. We report a low–molecular weight monomer whose supramolecular polymerization is triggered by the incorporation of water. The presence of water molecules as comonomers is essential to the polymerization process. The supramolecular polymeric material exhibits strong adhesion to surfaces, such as glass and paper. It can be used as a water-activated glue, which can be released at higher temperatures and reused many times without losing its performance.

INTRODUCTION

Structural water molecules that are buried inside proteins behave very differently from bulk water and often are integral parts of the folded protein structures (*1*). Experimental and theoretical evidence clearly demonstrates that this structural water forms strong, structure-stabilizing hydrogen bonds with polar groups incorporated in the surrounding proteins. Therefore, water molecules perform two important roles. On the one hand, they tighten the protein structures through additional bonding interactions; however, on the other hand, they also contribute to making the protein structure more flexible because of their reversible noncovalent binding (*2*, *3*). The concept and the importance of structural water as an essential constituent in protein folding are well acknowledged in biochemistry and cell biology (*4*).

Some fascinating examples about the application of structured water molecules as integral parts for the fabrication of supramolecular aggregates, including nanotubes (*5*), actuators (*6*), and polymers (*7*), have been reported, demonstrating the versatile role of water in material design and preparation. In the design of supramolecular polymers, an analogous concept of structural water appears to have been considered very rarely (*8*–*10*)—although water has been frequently used as a solvent for supramolecular polymerization (*8*, *9*). Compared to conventional polymers, supramolecular polymers (*10*–*13*) self-assemble from low–molecular weight monomers (LMWMs) by noncovalent interactions, thus opening the opportunity to easily design and incorporate functional elements into polymeric chain structures (*14*, *15*). Nevertheless, since the early example for supramolecular polymerization (*16*), studies use water molecules only as a solvent to disperse and solvate the monomers (*17*–*20*). Water itself has not yet been reported as an essential comonomer in supramolecular polymerization.

Here, we report an example of a supramolecular polymer containing water molecules taking the role of essential comonomers with great impact on the material properties and functions. The LMWM in this material is a triply benzo-21-crown-7 (B21C7)–substituted 1,3,5-benzenetricarboxamide (BTA) derivative (**TC7**; Fig. 1A) (*21*–*24*). Very much like structural water molecules in proteins, water molecules as comonomers efficiently induce and mediate unusual dynamics, flexibility, elasticity, and adhesive properties in the resulting functional supramolecular **TC7**-water copolymer.

RESULTS

Water absorption behavior

When dry, **TC7** is a fragile, nonsticky glass-like solid (Fig. 1C), and according to its powder x-ray diffraction (PXRD) pattern, the material is amorphous (fig. S15). The infrared (IR) spectrum of dry **TC7** together with the known assembly motif of BTA (fig. S16) indicate that **TC7** molecules self-assemble into one-dimensional supramolecular aggregates through amide-based H bonding (*21*, *23*, *24*). When dry **TC7** is exposed to air under ambient condition [25°C, relative humidity (RH), 40%], it quickly absorbs water and rapidly converts into a highly viscous soft material (less than 1 min). During water absorption, **TC7** gains at least 1.8% in weight and reaches an equilibrium state after ca. 10 min (fig. S18), as monitored by a microbalance. This behavior is unique because the structurally closely related controls **TC6** and **DC7** (Fig. 1B) show neither any weight growth nor the appearance of viscosity when exposed to air. More control compounds, with different crown ethers or cores, were further designed and applied (figs. S7 to S14). None of these control compounds display high viscosity and strong adhesion behavior when mixed with water, which shows BTA core-core hydrogen bonding to be as essential as the presence of B21C7 and the threefold symmetry of the compound. Other ring sizes (benzo-18-crown-6 and dibenzo-24-crown-8) or open-chain analogs do not show a similar adhesion behavior (see the Supplementary Information).

[1]College of Chemistry and Chemical Engineering, Hunan University, Changsha 410082, Hunan, P.R. China. [2]Bundesanstalt für Materialforschung und -prüfung (BAM), Unter den Eichen 87, 12205 Berlin, Germany. [3]School of Physics and Electronics, Hunan University, Changsha 410082, Hunan, P.R. China. [4]Department of Chemistry and Centre for Materials Discovery, University of Liverpool, Crown Street, Liverpool L69 7ZD, UK. [5]Institut Max von Laue–Paul Langevin, Large Scale Structures Group, 71 Avenue des Martyrs, 38042 Grenoble Cedex 9, France. [6]Stranski Laboratorium für Physikalische Chemie und Theoretische Chemie, Institut für Chemie, Technische Universität Berlin, Straße des 17. Juni 124, Sekr. TC7, D-10623 Berlin, Germany. [7]Institut für Chemie und Biochemie, Freie Universität Berlin, Takustrasse 3, 14195 Berlin, Germany. [8]Department of Pharmaceutical Engineering, China Pharmaceutical University, Nanjing 210009, P.R. China. [9]Sino-German Joint Research Lab for Space Biomaterials and Translational Technology, School of Life Sciences, Northwestern Polytechnical University, 127 Youyi Xilu, Xi'an, Shaanxi 710072, P.R. China.
*Corresponding author. Email: dongsy@hnu.edu.cn (S.D.); qi@nwpu.edu.cn (Z.Q.); c.schalley@fu-berlin.de (C.A.S.)

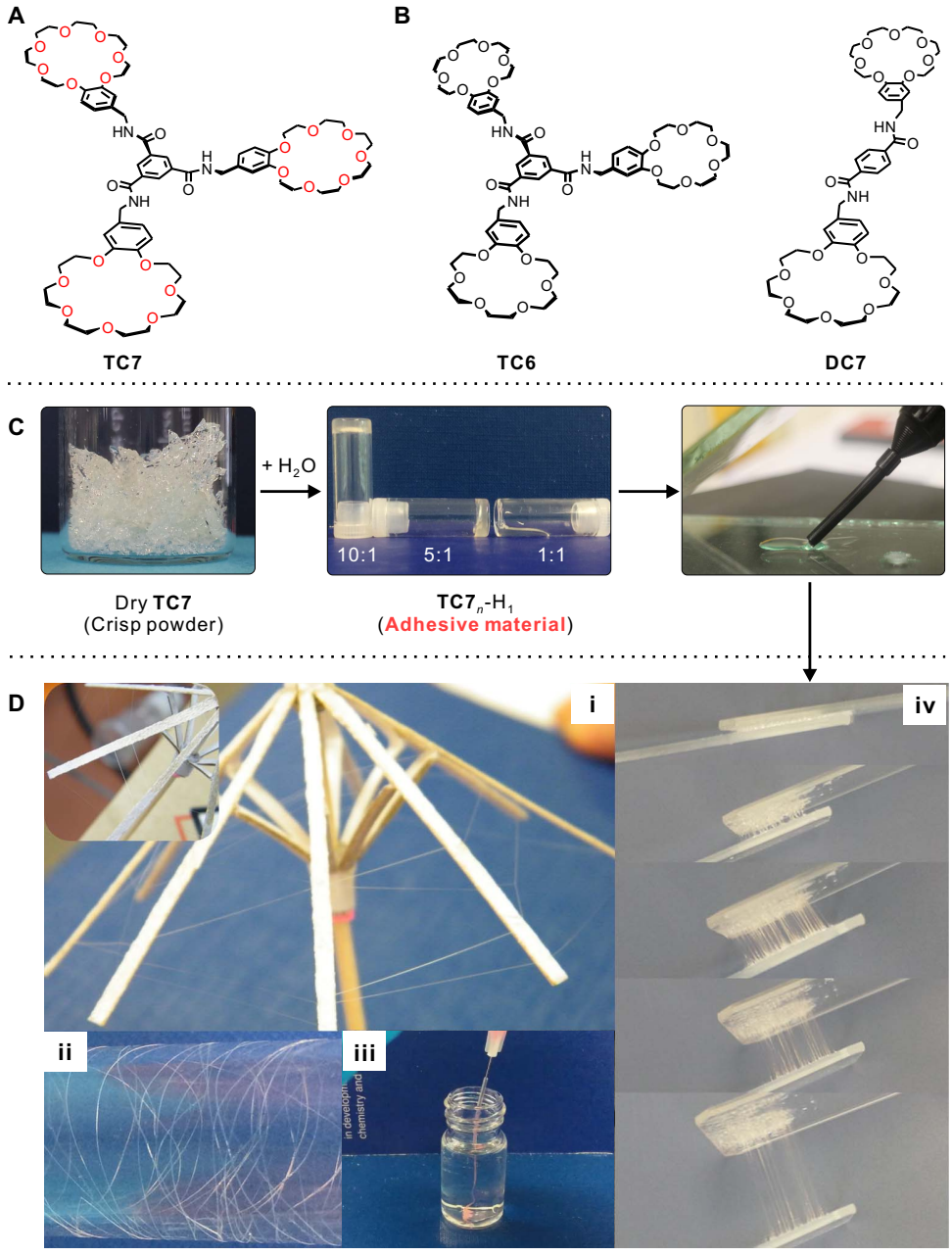

Fig. 1. Water-activated supramolecular polymerization. Chemical structures of (**A**) **TC7** and (**B**) the control compounds **TC6** and **DC7.** (**C**) Images of the **TC7** samples with different water content [$\mathbf{TC7}_n$-$\mathbf{H}_1$ is used to abbreviate samples with **TC7**: water (H) ratio of *n*: 1 (w/w)]. (**D**) Fibers drawn from $\mathbf{TC7}_{10}$-$\mathbf{H}_1$ (i and ii); fiber of $\mathbf{TC7}_3$-$\mathbf{H}_1$ injected to hexane (rhodamine B was added to the glue to make it clearly visible) (iii); fiber generated by coating glass slides with $\mathbf{TC7}_5$-$\mathbf{H}_1$ and then pulling them apart (at 80°C) (iv).

To test whether the water uptake is responsible for the drastic property changes, three **TC7** samples with different water content were prepared (Fig. 1C): $\mathbf{TC7}_{10}$-$\mathbf{H}_1$ (10:1, w/w), $\mathbf{TC7}_5$-$\mathbf{H}_1$ (5:1, w/w), and $\mathbf{TC7}_1$-$\mathbf{H}_1$ (1:1, w/w). As expected, water addition significantly changes the viscosity of the material: $\mathbf{TC7}_{10}$-$\mathbf{H}_1$ displays a very high viscosity and exhibits shape persistence, $\mathbf{TC7}_5$-$\mathbf{H}_1$ is a highly viscous glue-type liquid, and $\mathbf{TC7}_1$-$\mathbf{H}_1$ is a transparent less-viscous liquid that slowly flows when the test tube is tilted. Thus, water uptake dramatically alters the macroscopic appearance and the viscosity of the **TC7**-**H** materials. This transition between the dry solid and the viscous material states is fully reversible, indicating that the hydration and dehydration processes are also reversible.

Rheological characterization provides quantitative information on the storage moduli (G') and loss moduli (G'') of $\mathbf{TC7}_n$-$\mathbf{H}_1$ (n = 5, 10; fig. S20) as functions of angular frequency at fixed strain (1.0 %). Both samples behave as viscoelastic liquids for which the G' values are lower than the G'' values over the entire range of frequencies (*25*). In agreement with the macroscopic observation, $\mathbf{TC7}_{10}$-$\mathbf{H}_1$ is mechanically stronger than $\mathbf{TC7}_5$-$\mathbf{H}_1$: A G' value of 0.5 kPa and a zero-shear viscosity of 10^5 mPa·s were measured at 25°C. These values decrease significantly

when temperature increases from 25° to 40°C (fig. S22), exhibiting the thermosensitive nature of **TC7**-**H** materials.

Water addition also makes the resulting **TC7**-**H** materials easy to process. Thin and smooth fibers, with lengths up to several meters, were mechanically pulled from $\mathbf{TC7}_{10}$-$\mathbf{H}_1$ (Fig. 1D, fig. S20, and movie S1). They are quite flexible and can easily be rolled up on a small wooden umbrella (Fig. 1D) or—with much stronger curvature—wrapped around a capillary of 0.3-mm diameter (movie S2), thus providing evidence for high–molecular weight supramolecular polymeric structures (*26*). Fibers deposited on surfaces stayed intact over more than 6 months without any obvious cracking or agglomeration. For $\mathbf{TC7}_3$-$\mathbf{H}_1$, fibers and fibrous networks have also been successfully obtained by injection into hexane (movie S3). The material is sticky and bundles of parallel fibers can be pulled when the material is first deposited between two glass slides that are subsequently pulled apart (at 80°C; Fig. 1D), further proving good processability.

Structural elucidation of water molecules in polymers

To investigate the particular role of the water molecules incorporated in the **TC7**-**H** materials, attenuated total reflectance IR (ATR-IR) spectroscopy was performed (Fig. 2A and fig. S17). The spectrum of $\mathbf{TC7}_{10}$-$\mathbf{H}_1$ shows two strong bands at 3294 and 3509 cm^{-1} in the spectral areas characteristic for complexed and free amide NH groups (some supramolecular systems with complexed amide groups exhibit peaks for the N–H stretch vibration around 3200 to 3300 cm^{-1}) (*23*, *24*, *27*). Because overlap of O–H of water and N–H groups of **TC7** may occur (*28*), D_2O instead of H_2O was applied. In the spectrum of $\mathbf{TC7}_{10}$-$\mathbf{D}_1$, decreased intensities of bands at 3294 and at 3509 cm^{-1} are clearly visible (fig. S17), whereas a new band arises at 2505 cm^{-1}, which can be assigned to the D–O stretch vibrations of D_2O. The difference between the $\mathbf{TC7}_{10}$-$\mathbf{H}_1$ and $\mathbf{TC7}_{10}$-$\mathbf{D}_1$ samples indicates that the O–H band of H_2O overlaps with the NH band. This indicates the existence of hydrogen-bonded water molecules (for example, for solid phase of water ν_{as}O–H ~ 3200 cm^{-1} and ν_sO–H ~ 3400 cm^{-1}) (*29*). In principle, water could form H bonds with the polar O atom (in crown ether units) and/or the amide group (in cores). However, no noticeable H/D exchange between the NH groups and D_2O has been observed in a $\mathbf{TC7}_{10}$-$\mathbf{D}_1$ sample, and the proton signal of the NH group in the corresponding ^{1}H nuclear magnetic resonance (NMR) spectrum remains visible (Fig. 2B and fig. S23). This speaks against interactions between water molecules and the amide NH protons in $\mathbf{TC7}_{10}$-$\mathbf{D}_1$. That is, the water molecules in the $\mathbf{TC7}_{10}$-$\mathbf{H}_1$ material form H bonds more or less exclusively with O atoms of crown ethers.

Broadband dielectric spectroscopy (BDS) strongly supports the presence of water molecules as essential comonomers in the supramolecular polymer structure. The frequency dependence of the real part of the complex conductivity spectra of $\mathbf{TC7}_n$-$\mathbf{H}_1$ (n = 1, 2, 3, 4, 5, 10; fig. S26) corresponds to a typical conductivity-frequency behavior expected for semiconducting materials (fig. S27) (*30*). Their σ_{dc} values were obtained by fitting the Jonscher model and are displayed in Fig. 2C. For weight ratios of $\mathbf{TC7}_n$-$\mathbf{H}_1$ above $n \geq 3$, the resulting σ_{dc} over $1/T$ plots do not exhibit any discontinuity at around the freezing temperature of bulk water (Fig. 2C), indicating that up to this weight ratio, the supramolecular polymer does not contain significant amounts of free water molecules with bulk water properties. On the contrary, both $\mathbf{TC7}_2$-$\mathbf{H}_1$ and $\mathbf{TC7}_1$-$\mathbf{H}_1$ display a clearly visible discontinuity in the σ_{dc} over $1/T$ plots very close to the temperature at which also water displays such a discontinuity. This clearly points to the presence of significant amounts of free water molecules within the materials that freeze at the temperature at which the discontinuity is observed. In good agreement with these findings, an in situ single crystal structure of frozen water (fig. S28) is only obtained from the high–water content sample $\mathbf{TC7}_1$-$\mathbf{H}_1$ (*30*).

In addition, dielectric loss patterns were determined by BDS at −100°C. Figure 2D shows the frequency dependence of the dielectric loss at −100°C for $\mathbf{TC7}_n$-$\mathbf{H}_1$ ($n \geq 2$). The dry **TC7** sample displays a characteristic relaxation peak at a frequency around 10^3 Hz (maxima labeled in red), which is related to the molecular mobility of the **TC7** molecules. In addition, a new relaxation peak emerges at ca. 1 Hz (maxima labeled in pink) for the $\mathbf{TC7}_{10}$-$\mathbf{H}_1$ sample. This second peak can be assigned to the fluctuation of water molecules interacting with **TC7.** With increasing water content, the relaxation peak for the **TC7**-H_2O interaction shifts to higher frequencies and increases in intensity and finally superimposes that of the **TC7** molecules. Higher frequencies relate to higher molecular mobility, indicating weaker **TC7**-H_2O interactions with increasing water content. This behavior implies a lower viscosity for the **TC7**-H materials with higher water content (*31*), which is consistent with the macroscopic behavior discussed above ($\mathbf{TC7}_{10}$-H_1 has a higher viscosity than that of $\mathbf{TC7}_5$-H_1; Fig. 1C).

Density functional theory simulations for hydrogen-bonded geometries

To further investigate how these water molecules connect to **TC7**, we performed DFT simulations for various hydrogen-bonded geometries and calculated the averaged E_{HB} between crown ethers and water molecules, which are summarized in Fig. 2E and fig. S21. First, the model of crown ether units connected by one water molecule with a head-to-head geometry is considered, as indicated by the red circle dot. The E_{HB} is only ~0.1 eV, much weaker than that in liquid or frozen water. If the crown ether units are connected face to face by water molecules, then E_{HB} could gradually be enhanced as the number of N^{water} increases. Some representative complex structures are shown in Fig. 2E, and more are displayed in fig. S21. In Fig. 2E, we find that the more copolymerized water molecules are, the higher the E_{HB} is between crown ether units and center water molecules (upper triangles). When N^{water} between two crown ether units reaches 4 to 5, the E_{HB} increases to ~0.3 eV, close to the binding strength of hydrogen bonds in bulk ice I_h (blue horizontal lines in Fig. 2E) (*32*). We note that N^{water} per crown ether molecule of ~2.5 (4 to 5 water molecules between two crown ether units) roughly corresponds to the weight ratio of $\mathbf{TC7}_{10}$-$\mathbf{H}_1$. Further increasing N^{water} cannot enhance E_{HB} anymore. Instead, if more water molecules are introduced in this system, then water molecules will connect to each other or even form free bulk water clusters, as shown in fig. S29F (in this case, N^{water} is 8, corresponding to $\mathbf{TC7}_2$-$\mathbf{H}_1$).

On the basis of these findings from the BDS and the DFT simulations, we can conclude that the water molecules incorporated in the $\mathbf{TC7}_n$-$\mathbf{H}_1$ materials have two different roles: (i) For $n \geq 3$—mixtures that correspond to low water content—the water molecules are not free but act as essential comonomers to form high–molecular weight supramolecular polymers through hydrogen bonding with crown ether oxygen atoms, thus cross-linking the **TC7** stacks through hydrogen bonding. In line with the absence of H/D exchange reactions between incorporated D_2O and the **TC7** amide hydrogen atoms in $\mathbf{TC7}_{10}$-$\mathbf{H}_1$, our structural model may involve the formation of stacks of **TC7** molecules that are connected by amide-amide hydrogen bonding and π-stacking interactions, and these stacks are then cross-linked by water molecules (*33*). (ii) It is also demonstrated that the second role of incorporated water is that of water, which is not tightly bound to crown ether oxygen atoms and thus makes the polymeric structure flexible by

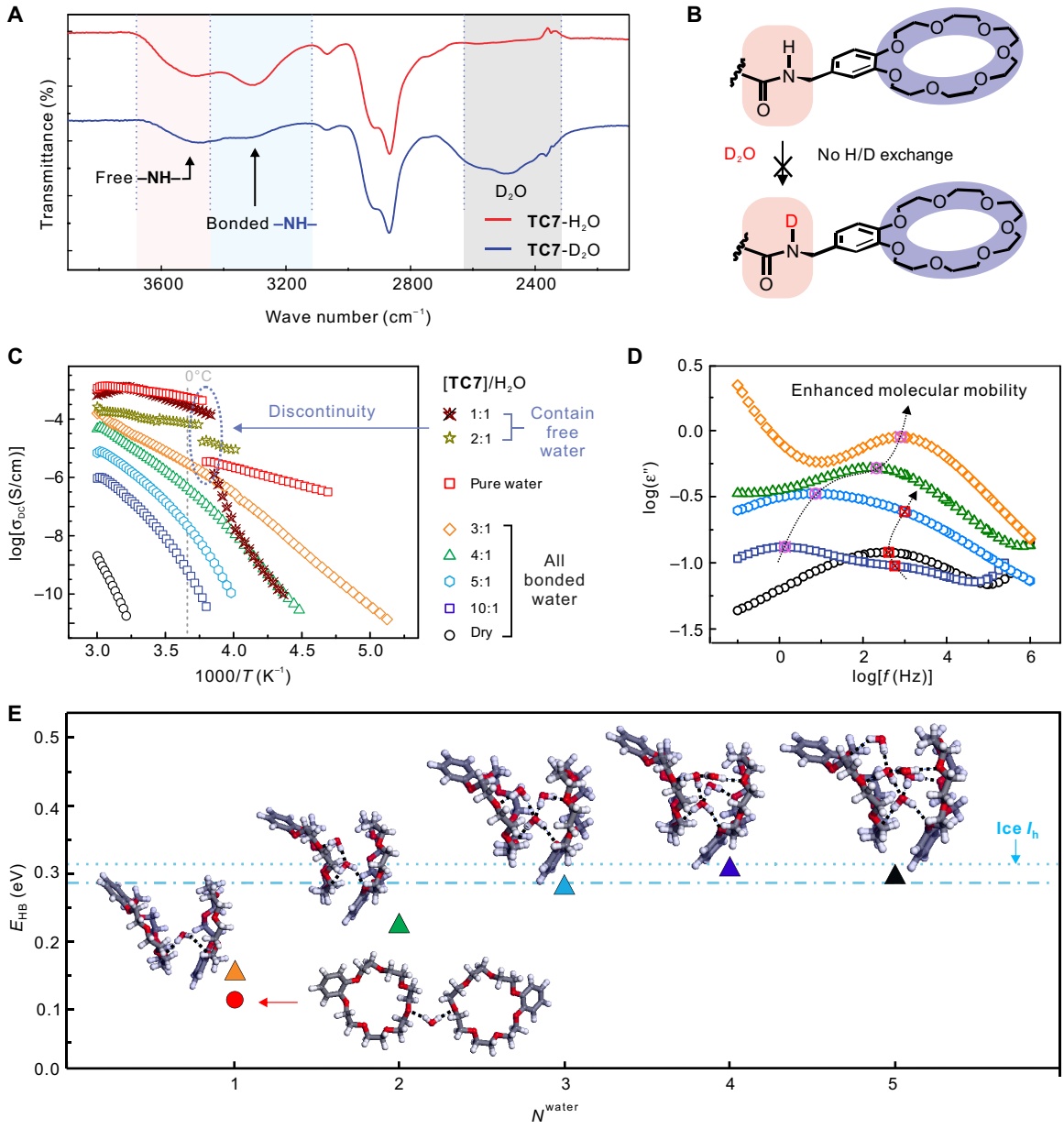

Fig. 2. The nature of water molecules in TC7-H materials. (**A**) ATR-IR spectra of **TC7** samples prepared with H_2O and D_2O (**TC7**$_{10}$-**H**$_1$ and **TC7**$_{10}$-**D**$_1$). (**B**) H/D exchange experiments conducted on **TC7**$_{10}$-**D**$_1$ adhesive (for details, see the Supplementary Materials). (**C**) The dependence of DC conductivity σ_{dc} versus $1/T$ for **TC7**-**H** materials with different water content. (**D**) Dielectric loss versus frequency for **TC7**-**H** materials with different water content at a temperature of −100°C: Frequency dependence of loss peaks due to hydrogen bonding between **TC7** and water (maxima labeled in pink) and between two adjacent **TC7** molecules (red labels). (**E**) Averaged hydrogen-bond strengths (E_{HB}) of crown ether–water systems with different number of water molecules (N^{water}) as obtained from the density functional theory (DFT) calculations: Some representative molecular structures are shown here (inserted chemical structures) and in fig. S26. The gray, red, and white spheres are carbon, oxygen, and hydrogen atoms, respectively. Hydrogen-bonds are indicated by short black-dashed lines. Blue horizontal–dashed and dot-dashed lines represent the theoretical and experimental E_{HB}'s of bulk ice I_h, respectively.

acting as a type of "lubricant." The higher water content, the more water molecules are available as lubricant water, and at high water content ($n \leq 2$), free water (bulky water clusters) is present, which can even form small ice crystals below 0°C detectable by crystallography.

This adhesive material is a typical supramolecular copolymer containing two comonomers (water and **TC7**) (*33*), with the water-crown ether-based hydrogen bonding and BTA core–based hydrogen bonding as the main driving forces. On the basis of the polymerization mechanism, it is also a solvent-free supramolecular polymerization process with water as an integral part of the copolymer.

Adhesion properties

Although the material investigated here is intriguing from a fundamental point of view because of the special role of water as essential comonomer, its utility for potential applications makes it even more interesting. The high viscosity and the strong tendency to form OH–O

hydrogen bonds between the crown ethers and the water molecules suggest that $\mathbf{TC7}_{10}$-$\mathbf{H}_1$ might be a powerful adhesive when attached to OH-terminated hydrophilic surfaces, such as glass or paper (*34*–*37*).

$\mathbf{TC7}_{10}$-$\mathbf{H}_1$ was deposited on a glass plate and processed by heating (for details, see the Supplementary Materials) to produce a uniform layer with a thickness of ca. 0.1 mm. Then, the second glass plate was pressed on that adhesive layer. The two plates adhered to each other immediately. This adhesion effect is stable for at least 24 months under ambient conditions (~25°C, 40 to 60 RH%) without a significant loss of the adhesive strength. Once two glass plates were adhered together, it is difficult to separate them. Weights up to 10 kg have been attached to one of the two slides, which were glued together on a 72-cm^2 area. No separation of the two slides by shear forces has been observed (Fig. 3A and movie S4). Forces perpendicular to the plane of the adhesive layer do not separate glass plates either (Fig. 3D and figs. S30 and S31), when an area of 10 cm^2 is used to glue the two slides to each other and a weight of 500 g is placed on the bottom slide. Similarly, $\mathbf{TC7}_{10}$-$\mathbf{H}_1$ exhibits a strong and long-lasting adhesion with other hydrophilic surfaces, including silicon wafers and paper. For example, two pieces of paper strips were easily glued to each other several seconds after a very small amount (less than 10 mg) of $\mathbf{TC7}_{10}$-$\mathbf{H}_1$ was placed on a 4.5-cm^2 area, followed by pressing the second paper strip onto it. This sample easily carries 2 kg in weight without detaching at the adhesive layer (Fig. 3C).

Pull-off adhesion tests were performed to quantitatively measure the adhesion strength of the $\mathbf{TC7}_{10}$-$\mathbf{H}_1$ coating to glass surfaces (Fig. 4 and fig. S31) (*27*, *38*, *39*). At a pull rate of 200 psi/s (1.38 MPa/s), the average adhesion strength is 602 psi (4.15 MPa) at 25°C (Fig. 4B). This value is much higher than those of previously reported supramolecular polymer adhesives (*19*, *27*). Commercially available PVA resulted in an adhesion strength of only 62 psi, only $^1/_{10}$ of that of $\mathbf{TC7}_{10}$-$\mathbf{H}_1$. With increasing temperature, the adhesion strength of our material decreases: At 40°, 50°, and 60°C, the corresponding adhesion strengths are 163, 92, and 60 psi (Fig. 4C), respectively. Consequently, the adhesion strength of $\mathbf{TC7}_{10}$-$\mathbf{H}_1$ at 60°C is still comparable to that of the commercial PVA glue at room temperature.

Tack tests of $\mathbf{TC7}_{10}$-$\mathbf{H}_1$ confirm strong interactions among **TC7** and water molecules (fig. S32). As the analysis criterion for the cohesive behavior, the maximum force is higher than 90 N at 25°C in the force-displacement diagram. $\mathbf{TC7}_{10}$-$\mathbf{H}_1$ has pronounced "secondary" and "tertiary" maxima, indicating a tack behavior with pronounced stringing and high energy required for separation. High temperature (60°C) leads not only to a great decay in the maximum force but also to the disappearance of the "tertiary maximum," indicating the weakening process of the cohesive behavior of $\mathbf{TC7}_{10}$-$\mathbf{H}_1$ materials at elevated temperature. Pull-off adhesion tests were also performed at different conditions, especially at low RH% and low temperature. At 20 RH%, the average adhesion strengths are 512, 472, and 293 psi at 20°, −10°, and −20°C (*39*), respectively. In vacuum, $\mathbf{TC7}_{10}$-$\mathbf{H}_1$ still shows strong adhesion behavior, with an average adhesion strength of 364 psi.

One might consider the decrease in adhesion strength with temperature as a disadvantage because it limits the temperature range of potential applications. However, this behavior can also be an advantage because the connection of the two pieces glued to each other with $\mathbf{TC7}_{10}$-$\mathbf{H}_1$ can be more easily released at higher temperature. This makes the adhesive reusable (*34*, *37*). To test the reusability, multiple cycles of pulling off the dolly, warming the material to 60°C, pressing the two glass slides together, and letting them rest for 20 min at room temperature were performed. After each cycle, another pulling test has been done. Even after 10 cycles, no substantial decrease has been observed in adhesion strength (Fig. 4D).

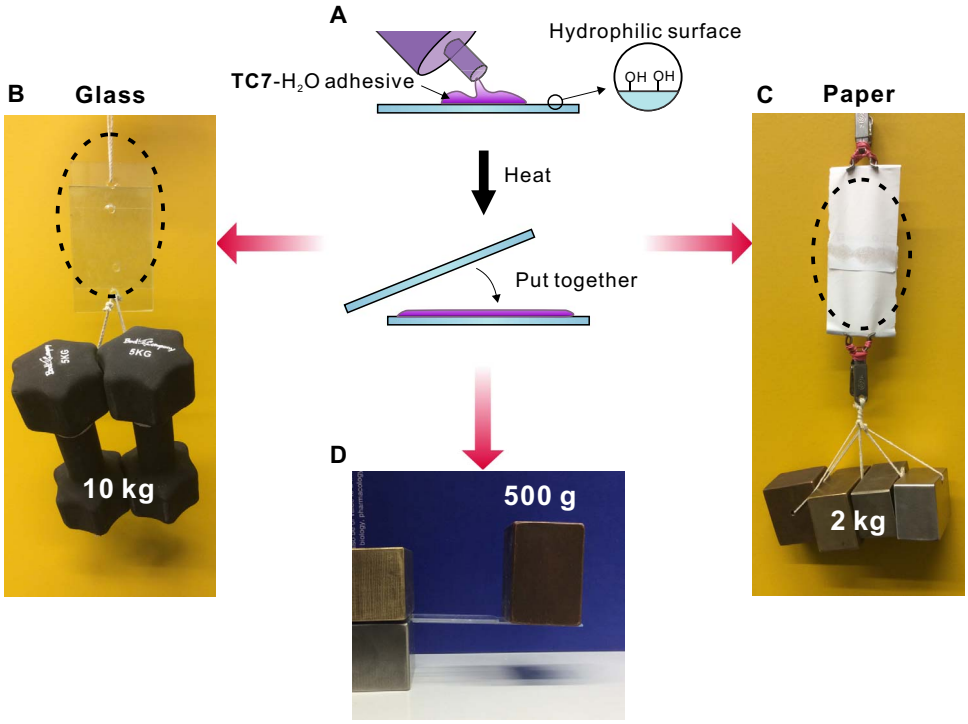

Fig. 3. Application of $\mathbf{TC7}_{10}$-$\mathbf{H}_1$ materials as adhesive materials. (**A**) A cartoon representation of the adhesion procedure. (**B** to **D**) Macroscopic adhesive behavior of $\mathbf{TC7}_{10}$-$\mathbf{H}_1$ materials on hydrophilic surface. The adhesion areas are 9.0 × 8.0 cm^2 (**B**), 4.5 × 1.0 cm^2 (**C**), and 4.0 × 2.5 cm^2 (**D**), respectively.

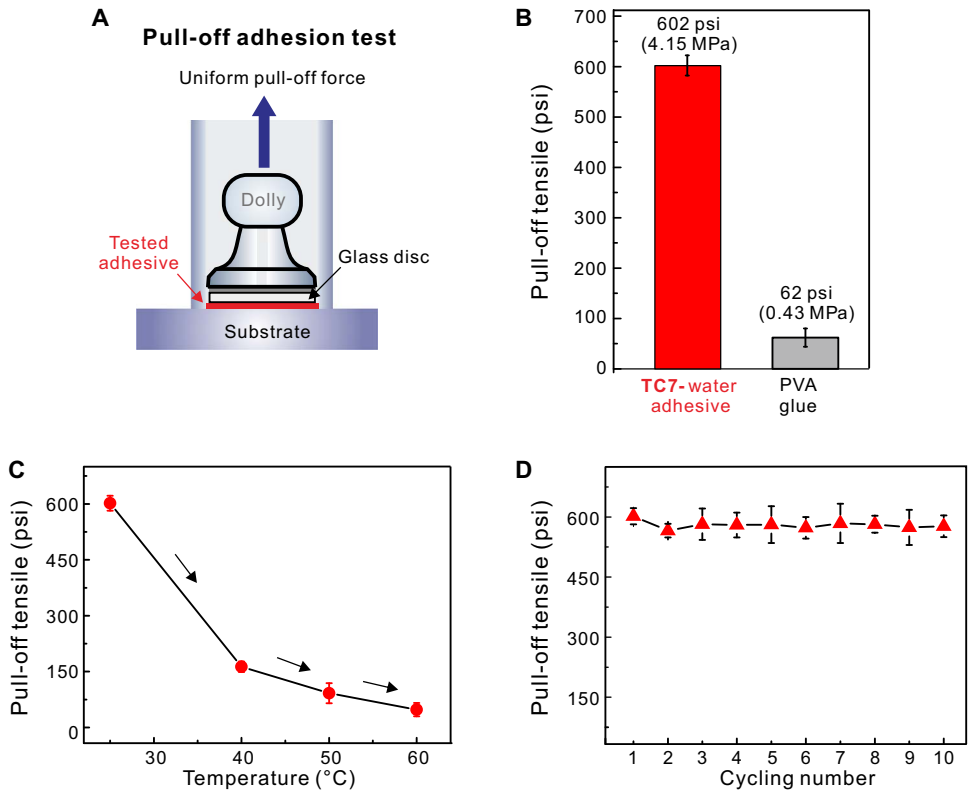

Fig. 4. Measurements of pull-off adhesion strength. (**A**) Illustration of the pull-off adhesion test. (**B**) Comparison of the adhesion effect of $\mathbf{TC7}_{10}$-$\mathbf{H}_1$ and commercially available adhesive poly(vinyl acetate) (PVA) glue at 25°C. (**C**) Adhesion strength of $\mathbf{TC7}_{10}$-$\mathbf{H}_1$ at different temperatures. (**D**) Recycling tests of $\mathbf{TC7}_{10}$-$\mathbf{H}_1$ at 25°C.

DISCUSSION

TC7 monomers themselves are stable under harsh conditions (for example, high temperature, high humidity, oxygen atmosphere, organic solvents atmospheres) and only starts to decompose above 350°C (fig. S33). When the $\mathbf{TC7}_{10}$-$\mathbf{H}_1$ adhesive material was placed between two glass slides and then exposed to air for more than two and a half years, no decay in adhesive performance was observed.

In conclusion, the triply crown ether–substituted **TC7** is interesting from a fundamental and from a point of view of potential applications. First, it represents an interesting supramolecular polymer in which water plays the role of an essential comonomer, whose incorporation causes dramatic property changes. Thus, water is important here far beyond being merely a solvent or being only responsible for hydrophobic effects that generate a driving force for supramolecular polymerization. Our experiments clearly indicate that the water molecules are hydrogen-bonded with the crown ether oxygen atoms to generate supramolecular polymers. Generally speaking, the incorporation of water in **TC7**-based materials produces an interesting adhesive material, which has a number of advantages: (i) Polymerization can occur at very high monomer concentrations, because even a small amount of water makes the material viscous, and solubility does not need to be considered. (ii) It is essentially a solvent-free polymerization (not only organic solvent-free), because all water molecules become constituents of supramolecular polymers. (iii) This adhesive material does not emit any toxic substances or unpleasant smell, because no organic solvent is required during the polymerization process or the preparation of the adhesive coating. (iv) The adhesion strength is high; nevertheless, the adhesive material can be reused by simply altering the temperature. Thus, the present work not only describes a successful resource-saving technology but also sheds new light on the fundamental importance of water in soft materials.

MATERIALS AND METHODS

All reagents were commercially available and used without further purification. Milli-Q water was used in all measurements. $\mathbf{BC7}$-$\mathbf{NH}_2$ was prepared by a reported method (*40*). NMR spectra were recorded with a Bruker AVANCE III-400 spectrophotometer, using the deuterated solvent as the lock and residual solvent or TMS as the internal reference. PXRD data were collected in transmission mode on samples held on thin Mylar film in aluminum well plates on a Panalytical X'Pert PRO MPD equipped with a high-throughput screening XYZ stage, x-ray focusing mirror, and PIXcel detector using Ni-filtered Cu Kα radiation. Data were measured over the range of 5° to 50° in ~0.013° steps over 60 min. A Sartorius microbalance CP2P was used for water sorption measurements. Mass spectra were obtained using an electrospray ionization interface on an Agilent LC/MSD TOF system. The height of the adhesive coating was determined on a Leica microscope (Primo Vert). Scanning electron microscopy (SEM) experiments were performed on a high-resolution HITACHI SU 8030 scanning electron microscope. Fourier-transform IR (FT-IR) spectra were recorded on a Nicolet Avatar 320 FT-IR. The thermograms of the adhesive materials were measured using differential scanning calorimetry (DSC; MDSC2910, TA Instruments). In the DSC measurements, the average of heating and cooling scans was at a scan rate of 10°C/min. A Thermo Fisher Scientific RS6000 rheometer with a plate-plate

geometry (diameter, 25 mm; gap, 1.5 mm) was used for the evaluation of G' and G''. Small-angle x-ray scattering (SAXS) measurements were carried out on a SAXSess mc2 small- and wide-angle scattering system (Anton Paar GmbH) with a sealed copper tube at $\lambda_{Cu\text{-}K\alpha}$ = 0.1542 nm with the option of line and point collimation. Single crystal x-ray data were collected on a Bruker APEX2 with microfocus-sealed x-ray tube (Mo Kα radiation, λ = 0.71073 Å, Bruker APEX2 area detector). Dielectric spectroscopy was carried out in a frequency range from 10^{-1} to 10^{6} Hz and between −100° and 60°C with a high-resolution ALPHA analyzer interfaced to an active sample head (Novocontrol). The measurements were carried out in parallel geometry. The temperature of the sample was controlled by a Quatro Novocontrol cryo-system with a stability of 0.1 K. To avoid the evaporation of water during the measurements, a sealed liquid parallel sample cell BDS 1308 (Novocontrol) was used. The adhesion strength measurements were performed on a pull-off adhesion tester (AT-A Automatic Adhesion Tester, PosiTest) (*41*). Tack tests were carried out on an Anton Paar Rheometer MCR102, with a plate-plate geometry (diameter, 25 mm; gap, 0.1 mm; and pull rate, 5 μm s^{-1}). Thermogravimetric analysis (TGA) was carried out using a TA Instruments Q5000IR analyzer with an automated vertical overhead thermobalance. The samples were heated at a rate of 5.0°C/min.

SUPPLEMENTARY MATERIALS

Supplementary material for this article is available at http://advances.sciencemag.org/cgi/content/full/3/11/eaao0900/DC1

Materials and Methods

scheme S1. Synthesis of **TC7** and control compounds.

scheme S2. Pull-off test of control compounds.

fig. S1. ^{1}H NMR spectrum (400 MHz, $CDCl_3$, 25°C) of **TC7.**

fig. S2. ^{13}C NMR spectrum (100 MHz, $CDCl_3$, 25°C) of **TC7.**

fig. S3. ^{1}H NMR spectrum (400 MHz, $CDCl_3$, 25°C) of **DC7.**

fig. S4. ^{13}C NMR spectrum (100 MHz, $CDCl_3$, 25°C) of **DC7.**

fig. S5. ^{1}H NMR spectrum (400 MHz, $CDCl_3$, 25°C) of **TC6.**

fig. S6. ^{13}C NMR spectrum (125 MHz, $CDCl_3$, 25°C) of **TC6.**

fig. S7. ^{1}H NMR spectrum (400 MHz, $CDCl_3$, 25°C) of **TC**-open.

fig. S8. ^{13}C NMR spectrum (125 MHz, $CDCl_3$, 25°C) of **TC**-open.

fig. S9. ^{1}H NMR spectrum (400 MHz, $CDCl_3$, 25°C) of **TC8.**

fig. S10. ^{1}H NMR spectrum (125 MHz, $CDCl_3$, 25°C) of **TC8.**

fig. S11. ^{13}C NMR spectrum (400 MHz, $CDCl_3$, 25°C) of **TCB.**

fig. S12. ^{1}H NMR spectrum (125 MHz, $CDCl_3$, 25°C) of **TCB.**

fig. S13. ^{1}H NMR spectrum (500 MHz, $CDCl_3$, 25°C) of **TC7A.**

fig. S14. ^{13}C NMR spectrum (125 MHz, $CDCl_3$, 25°C) of **TC7A.**

fig. S15. PXRD pattern of dry **TC7.**

fig. S16. IR spectrum of dry **TC7.**

fig. S17. IR spectra of $\mathbf{TC7}_{10}$-$\mathbf{H}_1$ and $\mathbf{TC7}_{10}$-$\mathbf{D}_1$.

fig. S18. Water absorbance curves of **TC7** under ambient conditions (25°C, 40% RH).

fig. S19. DSC measurements of $\mathbf{TC7}_{10}$-$\mathbf{H}_1$.

fig. S20. SEM images of $\mathbf{TC7}_{10}$-$\mathbf{H}_1$ adhesive.

fig. S21. Storage (G') and loss (G'') moduli of $\mathbf{TC7}_{10}$-$\mathbf{H}_1$ (red circles) and $\mathbf{TC7}_{5}$-$\mathbf{H}_1$ (blue circles) at 25°C.

fig. S22. Rheological performance of **TC7**-**H** materials at different temperatures.

fig. S23. H/D exchange experiments of $\mathbf{TC7}_{10}$-$\mathbf{D}_1$ adhesive.

fig. S24. SAXS of the $\mathbf{TC7}_{10}$-$\mathbf{H}_1$ adhesive at 25°C.

fig. S25. SAXS of the $\mathbf{TC7}_{1}$-$\mathbf{H}_1$ adhesive at 25°C.

fig. S26. The real part of the complex conductivity versus frequency of a $\mathbf{TC7}_{5}$-$\mathbf{H}_1$ adhesive at the indicated temperatures.

fig. S27. $[d \log \sigma_{dc} / dT]^{-1/2}$ versus T for **TC7**-**H** materials with different water contents.

fig. S28. H-bonding interactions between neighboring water molecules in the crystal structure of water (ice).

fig. S29. Detailed atomic structures of crown ether units connected by water molecules.

fig. S30. Tensile adhesion strength measurements of **TC7**-**H** adhesives.

fig. S31. Macroscopic tests of adhesion behavior of $\mathbf{TC7}_{10}$-$\mathbf{H}_1$.

fig. S32. Tack tests of $\mathbf{TC7}_{10}$-$\mathbf{H}_1$ adhesive at different temperature.

fig. S33. TGA measurements of **TC7**-**H** adhesive materials.

movie S1. Pulling a fiber from $\mathbf{TC7}_{10}$-$\mathbf{H}_1$ adhesive material.

movie S2. Fibers pulled from $\mathbf{TC7}_{10}$-$\mathbf{H}_1$ under optical microscopy.

movie S3. Injectable supramolecular adhesive from $\mathbf{TC7}_{3}$-$\mathbf{H}_1$.

movie S4. Macroscopic $\mathbf{TC7}_{10}$-$\mathbf{H}_1$ adhesion property.

References (*42*–*52*)

REFERENCES AND NOTES

1. M. Chaplin, Do we underestimate the importance of water in cell biology? *Nat. Rev. Mol. Cell Biol.* **7**, 861–866 (2006).
2. W. E. Royer, A. Pardanani, Q. H. Gibson, E. S. Peterson, J. M. Friedman, Ordered water molecules as key allosteric mediators in a cooperative dimeric hemoglobin. *Proc. Natl. Acad. Sci. U.S.A.* **93**, 14526–14531 (1996).
3. T. Sun, F.-H. Lin, R. L. Campbell, J. S. Allingham, P. L. Davies, An antifreeze protein folds with an interior network of more than 400 semi-clathrate waters. *Science* **343**, 795–798 (2014).
4. P. Ball, Water as an active constituent in cell biology. *Chem. Rev.* **108**, 74–108 (2008).
5. R. S. Johnson, T. Yamazaki, A. Kovalenko, H. Fenniri, Molecular basis for water-promoted supramolecular chirality inversion in helical rosette nanotubes. *J. Am. Chem. Soc.* **129**, 5735–5743 (2007).
6. H. Arazoe, D. Miyajima, K. Akaike, F. Araoka, E. Sato, T. Hikima, M. Kawamoto, T. Aida, An autonomous actuator driven by fluctuations in ambient humidity. *Nat. Mater.* **15**, 1084–1089 (2016).
7. M. Ma, L. Guo, D. G. Anderson, R. Langer, Bio-inspired polymer composite actuator and generator driven by water gradients. *Science* **339**, 186–189 (2013).
8. E. A. Appel, J. del Barrio, X. J. Loh, O. A. Scherman, Supramolecular polymeric hydrogels. *Chem. Soc. Rev.* **41**, 6195–6214 (2012).
9. A. Harada, *Supramolecular Polymer Chemistry* (Wiley-VCH, 2012).
10. L. Brunsveld, B. J. B. Folmer, E. W. Meijer, R. P. Sijbesma, Supramolecular polymers. *Chem. Rev.* **101**, 4071–4098 (2001).
11. T. Aida, E. W. Meijer, S. I. Stupp, Functional supramolecular polymers. *Science* **335**, 813–817 (2012).
12. X. Yan, F. Wang, B. Zheng, F. Huang, Stimuli-responsive supramolecular polymeric materials. *Chem. Soc. Rev.* **41**, 6042–6065 (2012).
13. G. L. Fiore, S. J. Rowan, C. Weder, Optically healable polymers. *Chem. Soc. Rev.* **42**, 7278–7288 (2013).
14. P. A. Korevaar, S. J. George, A. J. Markvoort, M. M. J. Smulders, P. A. J. Hilbers, A. P. H. J. Schenning, T. F. A. de Greef, E. W. Meijer, Pathway complexity in supramolecular polymerization. *Nature* **481**, 492–496 (2012).
15. J. Kang, D. Miyajima, T. Mori, Y. Inoue, Y. Itoh, T. Aida, A rational strategy for the realization of chain-growth supramolecular polymerization. *Science* **347**, 646–651 (2015).
16. C. Fouquey, J.-M. Lehn, A.-M. Levelut, Molecular recognition directed self-assembly of supramolecular liquid crystalline polymers from complementary chiral components. *Adv. Mater.* **2**, 254–257 (1990).
17. E. Krieg, M. M. C. Bastings, P. Besenius, B. Rybtchinski, Supramolecular polymers in aqueous media. *Chem. Rev.* **116**, 2414–2477 (2016).
18. M. Burnworth, L. Tang, J. R. Kumpfer, A. J. Duncan, F. L. Beyer, G. L. Fiore, S. J. Rowan, C. Weder, Optically healable supramolecular polymers. *Nature* **472**, 334–337 (2011).
19. A. S. Tayi, E. T. Pashuck, C. J. Newcomb, M. T. McClendon, S. I. Stupp, Electrospinning bioactive supramolecular polymers from water. *Biomacromolecules* **15**, 1323–1327 (2014).
20. X. Ma, H. Tian, Stimuli-responsive supramolecular polymers in aqueous solution. *Acc. Chem. Res.* **47**, 1971–1981 (2014).
21. S. Cantekin, T. F. A. de Greef, A. R. A. Palmans, Benzene-1,3,5-tricarboxamide: A versatile ordering moiety for supramolecular chemistry. *Chem. Soc. Rev.* **41**, 6125–6137 (2012).
22. C. Zhang, S. Li, J. Zhang, K. Zhu, N. Li, F. Huang, Benzo-21-crown-7/secondary dialkylammonium salt [2]pseudorotaxane- and [2]rotaxane-type threaded structures. *Org. Lett.* **9**, 5553–5556 (2007).
23. P. J. M. Stals, M. M. J. Smulders, R. Martín-Rapún, A. R. A. Palmans, E. W. Meijer, Asymmetrically substituted benzene-1,3,5-tricarboxamides: Self-assembly and odd-even effects in the solid state and in dilute solution. *Chemistry* **15**, 2071–2080 (2009).
24. P. J. M. Stals, J. C. Everts, R. de Bruijn, I. A. W. Filot, M. M. J. Smulders, R. Martín-Rapún, E. A. Pidko, T. F. A. de Greef, A. R. A. Palmans, E. W. Meijer, Dynamic supramolecular polymers based on benzene-1,3,5-tricarboxamides: The influence of amide connectivity on aggregate stability and amplification of chirality. *Chemistry* **16**, 810–821 (2010).
25. M. Tokita, K. Nishinari, Eds., *Gel: Structures, Properties, and Functions: Fundamentals and Applications* (Springer, 2009).
26. H. W. Gibson, N. Yamaguchi, J. W. Jones, Supramolecular pseudorotaxane polymers from complementary pairs of homoditopic molecules. *J. Am. Chem. Soc.* **125**, 3522–3533 (2003).

27. J. Courtois, I. Baroudi, N. Nouvel, E. Degrandi, S. Pensec, G. Ducouret, C. Chanéac, L. Bouteiller, C. Creton, Supramolecular soft adhesive materials. *Adv. Funct. Mater.* **20**, 1803–1811 (2010).
28. B. I. El-Eswed, M. B. Zughul, G. A. W. Derwish, Infrared spectroscopic study of the role of water in crown ethers and their molecular complexes with 3- and 4-nitrophenol. *J. Incl. Phenom. Macrocycl. Chem.* **28**, 245–258 (1997).
29. A. Rustenholtz, J. L. Fulton, C. M. Wai, An FT-IR study of crown ether–water complexation in supercritical CO_2. *J. Phys. Chem. A* **107**, 11239–11244 (2003).
30. F. Kremer, A. Schönhals, Eds., *Broadband Dielectric Spectroscopy* (Springer, 2002).
31. A. Kyritsis, P. Pissis, J. Grammatikakis, Dielectric relaxation spectroscopy in poly (hydroxyethyl acrylates)/water hydrogels. *J. Polym. Sci. B Polym. Phys.* **33**, 1737–1750 (1995).
32. I. Hamada, A van der Waals density functional study of ice Ih. *J. Chem. Phys.* **133**, 214503 (2010).
33. T. F. A. de Greef, E. W. Meijer, Materials science: Supramolecular polymers. *Nature* **453**, 171–173 (2008).
34. C. Heinzmann, C. Weder, L. M. de Espinosa, Supramolecular polymer adhesives: Advanced materials inspired by nature. *Chem. Soc. Rev.* **45**, 342–358 (2016).
35. H. Lee, B. P. Lee, P. B. Messersmith, A reversible wet/dry adhesive inspired by mussels and geckos. *Nature* **448**, 338–341 (2007).
36. Q. Zhao, D. W. Lee, B. K. Ahn, S. Seo, Y. Kaufman, J. N. Israelachvili, J. H. Waite, Underwater contact adhesion and microarchitecture in polyelectrolyte complexes actuated by solvent exchange. *Nat. Mater.* **15**, 407–412 (2016).
37. G. P. Maier, M. V. Rapp, J. H. Waite, J. N. Israelachvili, A. Butler, Adaptive synergy between catechol and lysine promotes wet adhesion by surface salt displacement. *Science* **349**, 628–632 (2015).
38. H. Lakrout, P. Sergot, C. Creton, Direct observation of cavitation and fibrillation in a probe tack experiment on model acrylic pressure-sensitive-adhesives. *J. Adhes.* **69**, 307–359 (1999).
39. D. A. Dillard, A. V. Pocius, Eds., *The Mechanics of Adhesion* (Elsevier Science, 2002).
40. Z. Qi, P. M. de Molina, W. Jiang, Q. Wang, K. Nowosinski, A. Schulz, M. Gradzielski, C. A. Schalley, Systems chemistry: Logic gates based on the stimuli-responsive gel–sol transition of a crown ether-functionalized bis(urea) gelator. *Chem. Sci.* **3**, 2073–2082 (2012).
41. Paints and Varnishes — Pull-Off Test for Adhesion ISO 4624:2002 (2002).
42. G. M. Sheldrick, *SHELXT* - Integrated space-group and crystal-structure determination. *Acta Crystallogr. A Found. Adv.* **71**, 3–8 (2015).
43. G. M. Sheldrick, Crystal structure refinement with *SHELXL*. *Acta Crystallogr. C Struct. Chem.* **71**, 3–8 (2015).
44. O. V. Dolomanov, L. J. Bourhis, R. J. Gildea, J. A. K. Howard, H. Puschmann, *OLEX2*: A complete structure solution, refinement and analysis program. *J. Appl. Crystallogr.* **42**, 339–341 (2009).
45. G. Kresse, J. Hafner, Ab initio molecular dynamics for liquid metals. *Phys. Rev. B* **47**, 558–561 (1993).
46. G. Kresse, J. Hafner, Ab initio molecular-dynamics simulation of the liquid-metal–amorphous-semiconductor transition in germanium. *Phys. Rev. B* **49**, 14251–14269 (1994).
47. J. Klimeš, D. R. Bowler, A. Michaelides, Chemical accuracy for the van der Waals density functional. *J. Phys. Condens. Matter* **22**, 022201 (2009).
48. X. Yan, D. Xu, X. Chi, J. Chen, S. Dong, X. Ding, Y. Yu, F. Huang, A multiresponsive, shape-persistent, and elastic supramolecular polymer network gel constructed by orthogonal self-assembly. *Adv. Mater.* **24**, 362–369 (2012).
49. S. Dong, X. Yan, B. Zheng, J. Chen, X. Ding, Y. Yu, D. Xu, M. Zhang, F. Huang, A supramolecular polymer blend containing two different supramolecular polymers through self-sorting organization of two heteroditopic monomers. *Chemistry* **18**, 4195–4199 (2012).
50. F. Wang, J. Zhang, X. Ding, S. Dong, M. Liu, B. Zheng, S. Li, L. Wu, Y. Yu, H. W. Gibson, F. Huang, Metal coordination mediated reversible conversion between linear and cross-linked supramolecular polymers. *Angew. Chem. Int. Ed.* **49**, 1090–1094 (2010).
51. S. Dong, L. Gao, J. Li, D. Xu, Q. Zhou, Photo-responsive linear and cross-linked supramolecular polymers based on host–guest interactions. *Polym. Chem.* **4**, 3968–3973 (2013).
52. A. Lopez, E. Degrandi-Contraires, E. Canetta, C. Creton, J. L. Keddie, J. M. Asua, Waterborne polyurethane-acrylic hybrid nanoparticles by miniemulsion polymerization: Applications in pressure-sensitive adhesives. *Langmuir* **27**, 3878–3888 (2011).

Acknowledgments: We are grateful for the computational resources provided by the National Supercomputing Center in Changsha. We thank R. Haag for the discussions and Z. Zhong for the pull-off tests. **Funding:** S.D. thanks the Fundamental Research Funds for the Central Universities from Hunan University and the Alexander von Humboldt Foundation for financial support. Z.Q. acknowledges financial support from the Thousand Talents Program and Northwestern Polytechnical University of China (1800-16GH030121). C.A.S. is grateful to the Deutsche Forschungsgemeinschaft (CRC 765) for funding. Y.F. is supported by the National Natural Science Foundation of China under grant nos. 11604092 and 11634001. M.L. and C.J.S. acknowledge funding from the Engineering and Physical Sciences Research Council (EP/N004884/1) and the European Research Council under the European Union's Seventh Framework Programme (FP/2007-2013) through grant agreement no. 321156 (ERC-AG-PE5-ROBOT). **Author contributions:** S.D., Z.Q., and C.A.S. designed and directed the study. J.L. and A.S. performed the BDS. Y.F. performed the DFT calculation. M.L. and C.J.S. performed the crystal structure, PXRD, and TGA. L.C. performed the SAXS experiments. L.G. and W.C. performed the H/D experiments and pull-off adhesion tests. J.L. and J.S. performed the compound design, synthesis, and pull-off adhesion tests. S.D., Z.Q., and C.A.S. wrote the manuscript. All the authors commented on the paper. **Competing interest:** All authors declare that they have no competing interests. S.D. and Z.Q. claim responsibility for all the figures in the main text and the Supplementary Materials. **Data and materials availability:** All data needed to evaluate the conclusions in the paper are present in the paper and/or the Supplementary Materials. Additional data related to this paper may be requested from the authors.

Submitted 13 June 2017
Accepted 27 October 2017
Published 15 November 2017
10.1126/sciadv.aao0900

Citation: S. Dong, J. Leng, Y. Feng, M. Liu, C. J. Stackhouse, A. Schönhals, L. Chiappisi, L. Gao, W. Chen, J. Shang, L. Jin, Z. Qi, C. A. Schalley, Structural water as an essential comonomer in supramolecular polymerization. *Sci. Adv.* **3**, eaao0900 (2017).

Science Advances

Structural water as an essential comonomer in supramolecular polymerization

Shengyi Dong, Jing Leng, Yexin Feng, Ming Liu, Chloe J. Stackhouse, Andreas Schönhals, Leonardo Chiappisi, Lingyan Gao, Wei Chen, Jie Shang, Lin Jin, Zhenhui Qi and Christoph A. Schalley

Sci Adv **3** (11), eaao0900.
DOI: 10.1126/sciadv.aao0900